# -Supporting information-

## Simultaneous facilitation of $CO_2$ adsorption and proton feeding in $Bi/Bi_2O_3$ heterostructure nanosheets for enhanced electroreduction of $CO_2$ to formate in a wide potential window

Wenwen Wang [a], Guangyu Ruan [a], Xin Wang [a], Chao Wu [a], Qinian Wang [a,b]*

[a] School of Resources and Environmental Engineering, Anhui University, Hefei, Anhui, 230601, China

[b] Anhui Province Key Laboratory of Wetland Ecosystem Protection and Restoration, Anhui University, Hefei, Anhui, 230601, China

* Corresponding Authors;

Phone: (86) 551 63861441; Fax: (86) 551 63861441; E−mail: wqn88@126.com (Q. Wang).

Address: School of Resources and Environmental Engineering, Anhui University, Hefei, 230601, China

## Table of Contents

**Table S1.** Summary of the recent reports on ERCF using Bi-based catalysts in a H-type cell.

| Catalysts | Electrolyte | $FE_{formate}$ (%) | $j_{formate}$ (mA cm$^{-2}$ ) | Potential window (mV; $FE_{formate}$ > 90 %) | Refs |
|---|---|---|---|---|---|
| Bi nanotubes | 0.5 M $KHCO_3$ -1.22 V vs. RHE | 90 | 48 | 450 | [1] |
| $Bi_2O_3$ nanotubes | 0.5 M $KHCO_3$ -1.05 V vs. RHE | 90 | 60 | 300 | [2] |
| $Bi_2O_3$ NSs@MCCM | 0.1 M $KHCO_3$ -1.355 V vs. RHE | 90 | 17.7 | 300 | [3] |
| Mesoporous Bi NSs | 0.5 M $KHCO_3$ -1.05 V vs. RHE | 82 | 17 | 240 | [4] |
| $Bi_2O_3$@C | 0.5 M $KHCO_3$ -0.9 V vs. RHE | 92 | 7.5 | 100 | [5] |
| $Bi_2O_3$@C-800 | 0.5 M $KHCO_3$ -0.9 V vs. RHE | 92.0 | 7.5 | 200 | [6] |
| Bi MSs | 0.1 M $KHCO_3$ -1.0 V vs. RHE | 96.2 | 5.08 | 500 | [7] |
| Bi nanostructure | 0.5 M $KHCO_3$ -0.9 V vs. RHE | 92 | 15 | 100 | [8] |
| PD-Bi1 | 0.5 M $KHCO_3$ -0.9 V vs. RHE | 91.4 | 7 | 100 | [9] |
| Bi-MOF | 0.5 M $KHCO_3$ -0.9 V vs. RHE | 92.2 | 4.5 | 300 | [10] |
| Bi-nanosheets | 0.5 M $KHCO_3$ -0.9 V vs. RHE | 92 | 10.5 | 300 | [11] |
| SOR Bi@C NPs | 0.5 M $KHCO_3$ -0.99 V vs. RHE | 95 | 10.5 | 440 | [12] |
| Bi RDs | 0.5 M $KHCO_3$ -0.7 V vs. RHE | 93.5 | 1.5 | 500 | [13] |
| POD-Bi | 0.5 M $KHCO_3$ -1.16 V vs. RHE | 95 | 52.8 | 300 | [14] |
| Bi (btb) | 0.5 M $KHCO_3$ -0.97 V vs. RHE | 95 | 5 | 200 | [15] |
| Bi/$Bi_2O_3$-NSs | 0.5 M $KHCO_3$ -0.87 V vs. RHE | 90.4 | 33 | 100 | [16] |
| $Bi_2S_3$-$Bi_2O_3$ NSs | 0.1 M $KHCO_3$ -1.1 V vs. RHE | 93.8 | 17.1 | 400 | [17] |
| Bi NSs | 0.5 M $KHCO_3$ -0.96 V vs. RHE | 76.67 | 60.22 | 100 | This work |
| Bi/$Bi_2O_3$ NSs | 0.5 M $KHCO_3$ -0.96 V vs. RHE | 96.45 | 70.27 | 800 | This work |

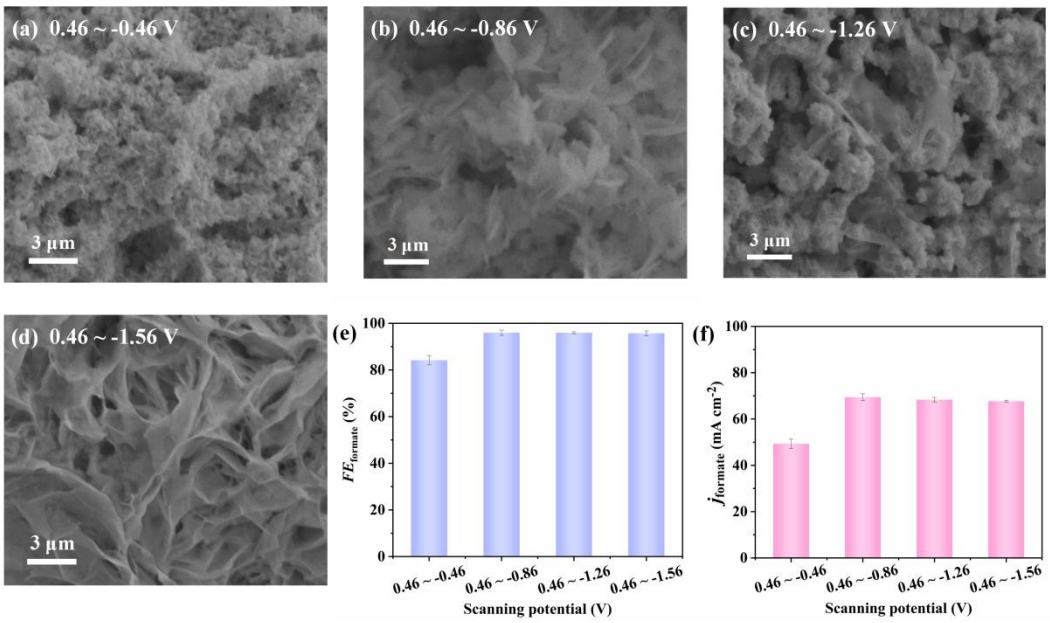


**Fig. S1**. Influences of the potential range for the reduction of the as-prepared $Bi_2O_3$ NSs on the morphology and ERCF performance of the formed nanosheets. Scan number was 10, and the applied potential for ERCF was −0.96 V. The highest $FE_{\text{formate}}$ and $j_{\text{formate}}$ were obtained when the potential range was 0.46 ~ −0.86 V.

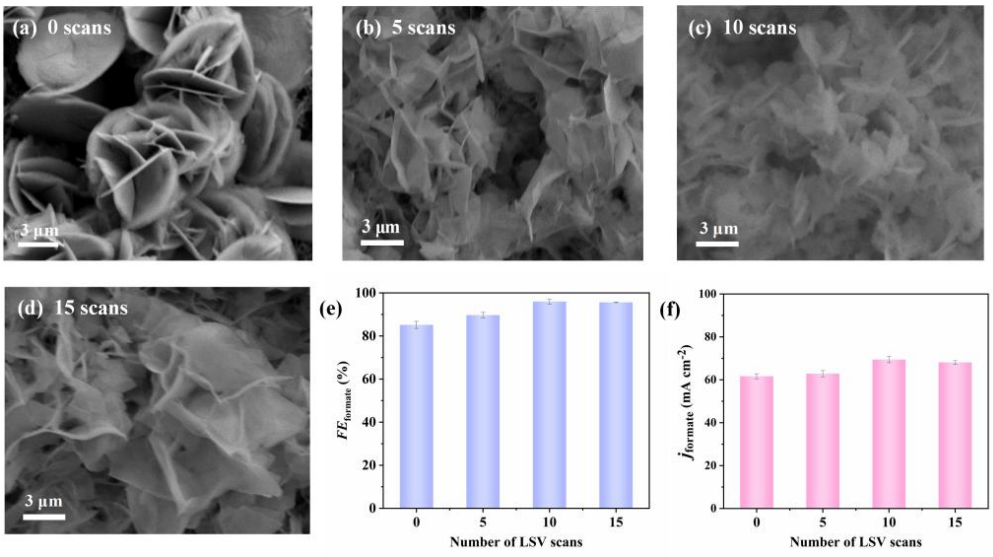


**Fig. S2.** Influences of the scan number for the reduction of the as-prepared $Bi_2O_3$ NSs on the morphology and ERCF performance of the formed nanosheets. Potential range was 0.46 ~ −0.86 V, and the applied potential for ERCF was −0.96 V. The highest $FE_{formate}$ and $j_{formate}$ was obtained when the scan number was 10.

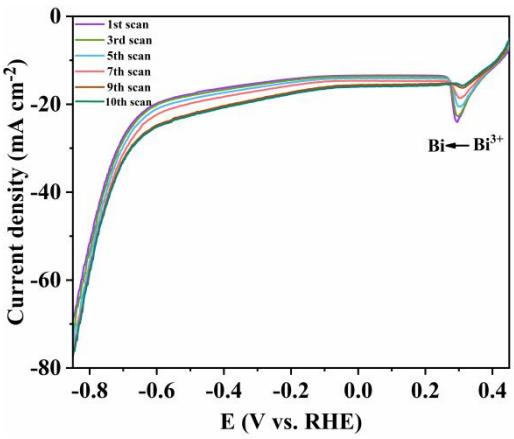


**Fig. S3.** Cycle-dependent LSV curves of $Bi_2O_3$ in a $CO_2$-saturated 0.5 M $KHCO_3$ solution. The potential range was 0.46 ~ −0.86 V.

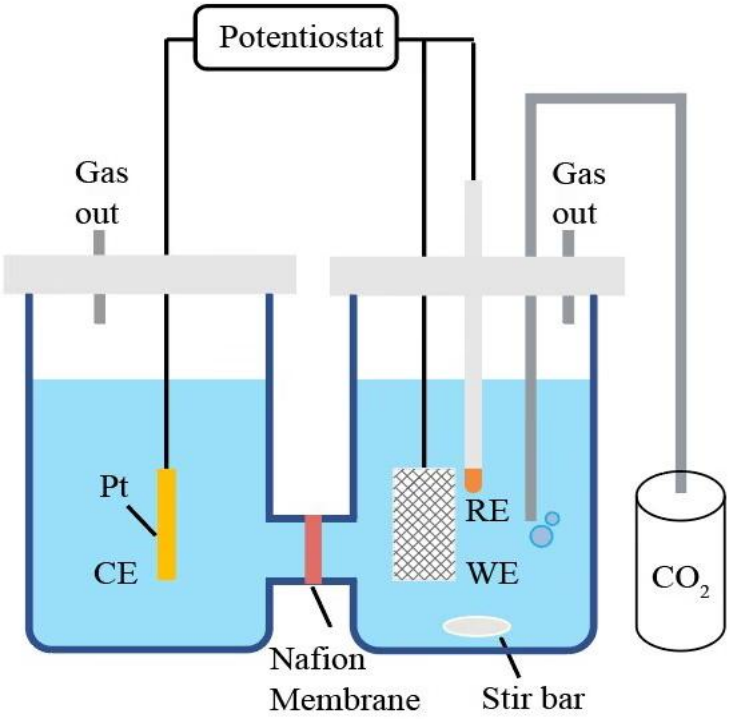


**Fig. S4**. Scheme of the self-assembled electrolysis reactor for electrochemical experiments. WE: working electrode, RE: reference electrode, CE: counter electrode.

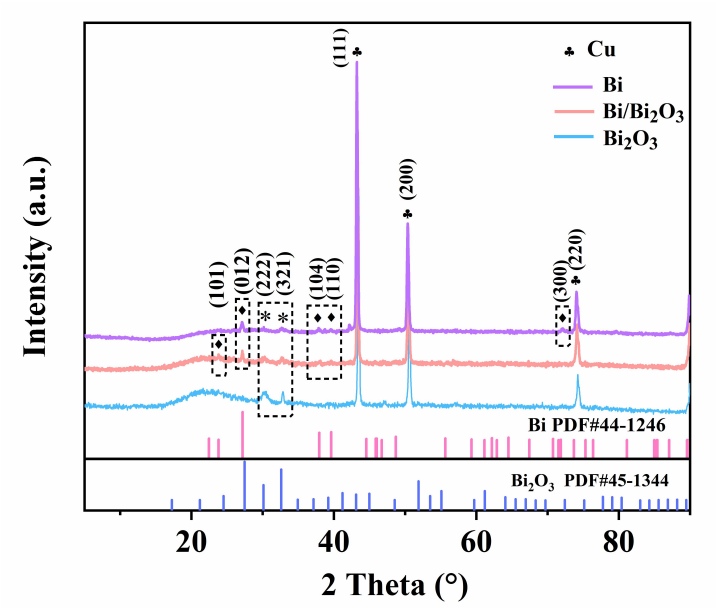


**Fig. S5.** XRD patterns of Bi, $Bi_2O_3$, and Bi/$Bi_2O_3$ samples.

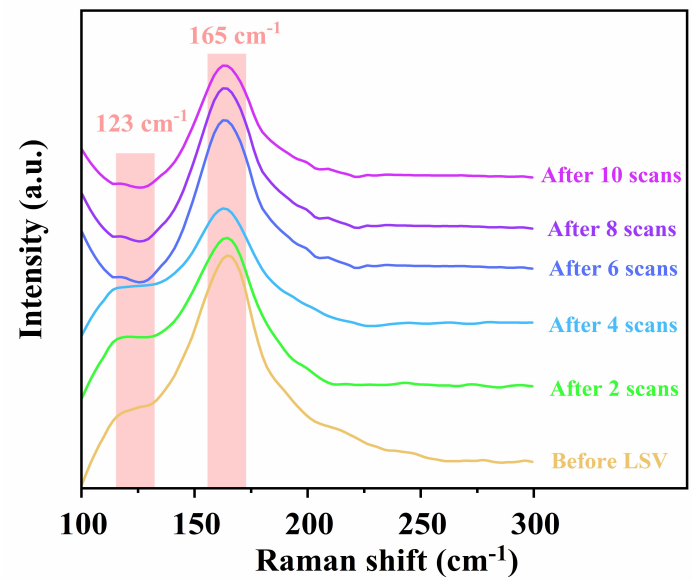


**Fig. S6.** *In situ* Raman spectra of $Bi_2O_3$ NSs before and after different LSV scans in a $CO_2$-saturated 0.5 M $KHCO_3$ solution.

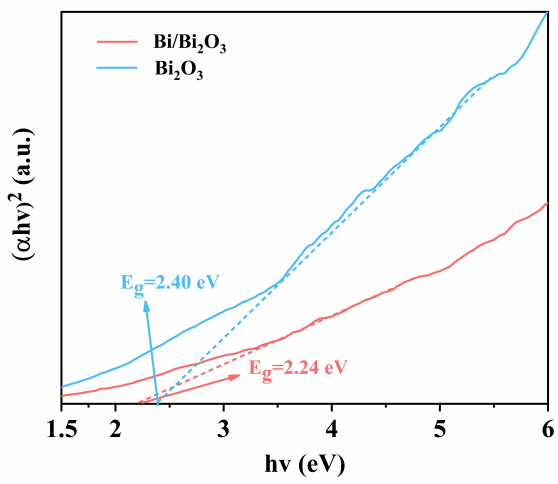


**Fig. S7.** Tauc plots for the as-prepared samples. The Eg of the as-prepared sample was obtained by fitting the Kubelka-Munk formula.[18] The Eg values of $Bi_2O_3$ NSs and $Bi/Bi_2O_3$ hybrid NSs were 2.40 and 2.24 eV, respectively.

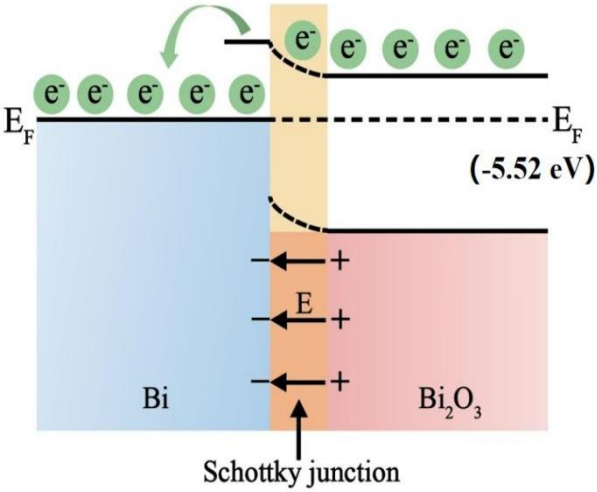


**Fig. S8.** Schematic illustration of the charge transfer process in $Bi/Bi_2O_3$ hybrid NSs.

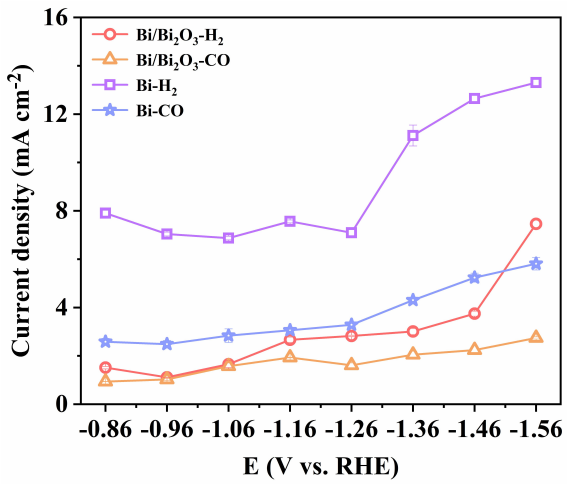


**Fig. S9.** Current density of different gas products ($H_2$, CO).

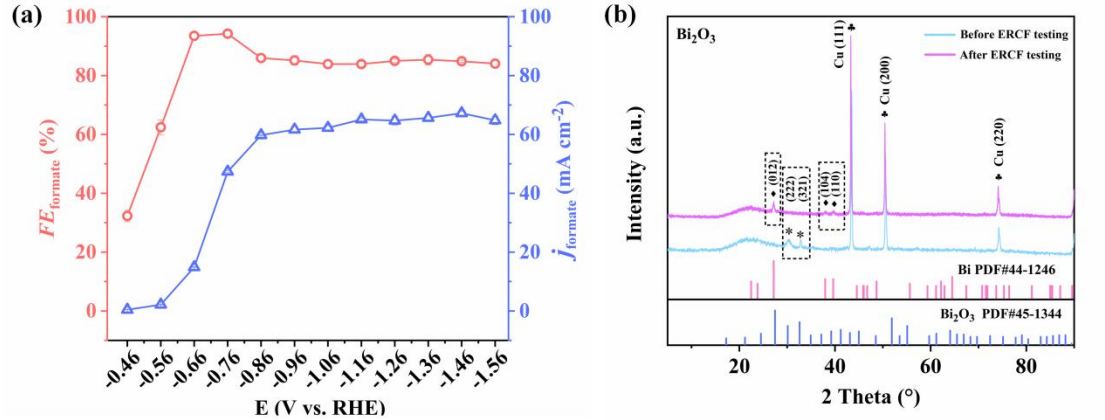


**Fig. S10.** (a) ERCF performance of $Bi_2O_3$ at different cathode potentials and (b) XRD patterns of $Bi_2O_3$ sample before and after ERCF testing at −0.96 V.

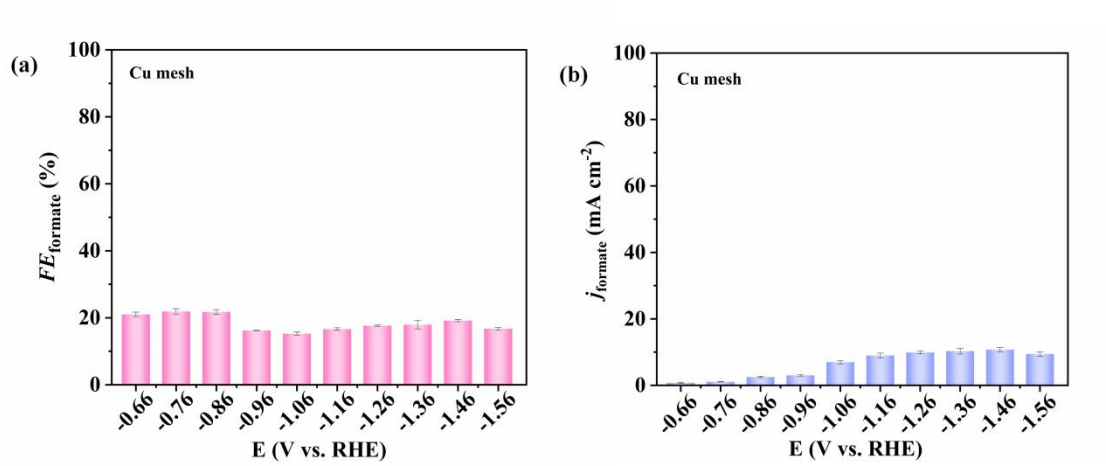


**Fig. S11.** ERCF performance of the Cu mesh at different cathode potentials.

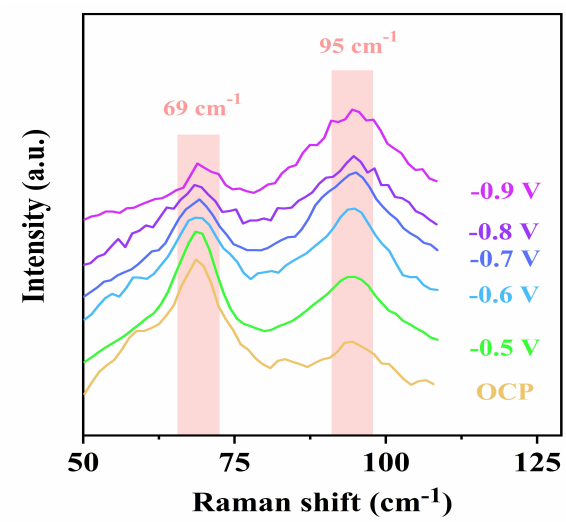


**Fig. S12.** *Ex situ* Raman spectra of the $Bi/Bi_2O_3$ hybrid NSs as a function of the applied potential.

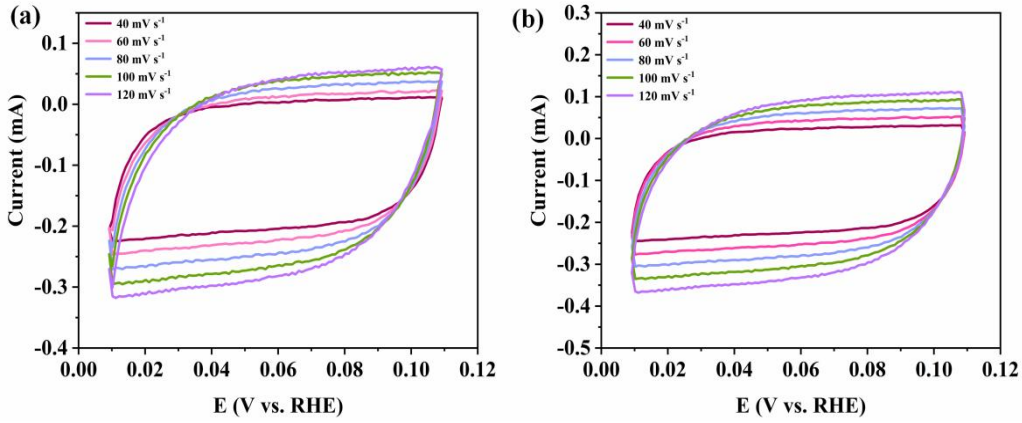


**Fig. S13.** CV curves of (a) Bi NSs and (b) Bi/$Bi_2O_3$ hybrid NSs at different scan rates in the range of 40 to 120 mV $s^{-2}$, recorded in a $N_2$-saturated 0.5 M $KHCO_3$ solution. The plot of the current density at a specific potential against scan rate has a linear relationship, and the slope gives the electrochemical double-layer capacitance ($C_{dl}$).

The electrochemical active surface areas (ECSA) was calculated by the formula: ECSA = $C_{dl} \times A/C_0$, where $C_{dl}$ is the specific capacitance of the fabricated catalysts, $C_0$ is the specific capacitance of a flat standard electrode with 1 $cm^2$ of real surface area ($C_0$ = 40 μF $cm^{-2}$ [19]), and $A$ is the geometric area. The ECSA of Bi NSs and Bi/$Bi_2O_3$ NSs hybrids were estimated to be 44.75 and 37.50 $cm^2$.

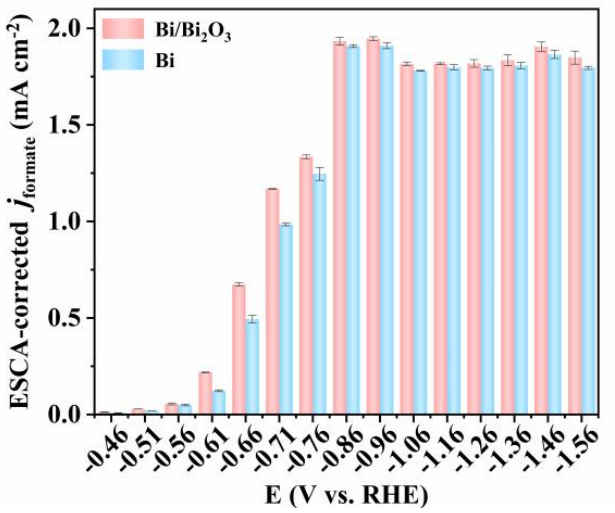


**Fig. S14.** ESCA-normalised current density for formate production.

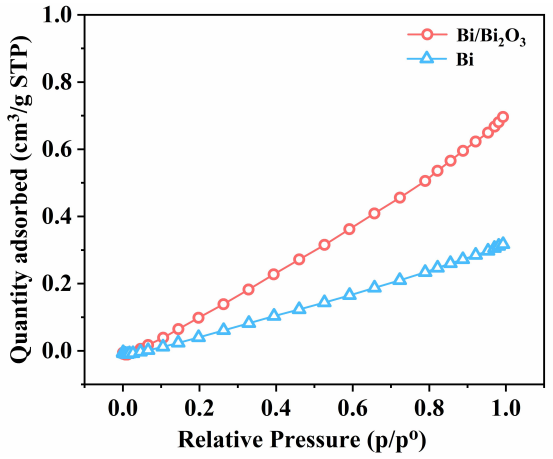


**Fig. S15.** $CO_2$ adsorption isotherms of Bi NSs and $Bi/Bi_2O_3$ hybrid NSs.

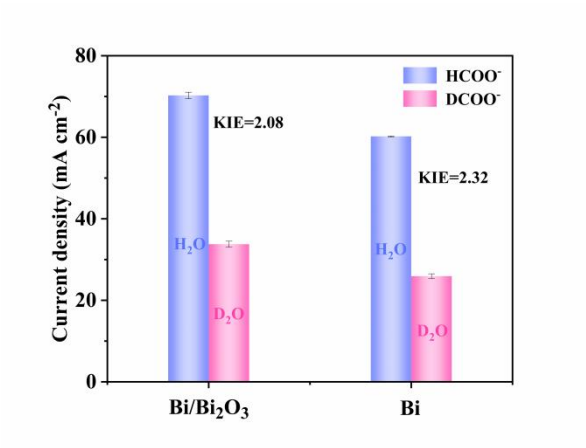


**Fig. S16.** Kinetic isotopic effect of H/D over the Bi NSs and $Bi/Bi_2O_3$ hybrid NSs catalysts at −0.96 V.

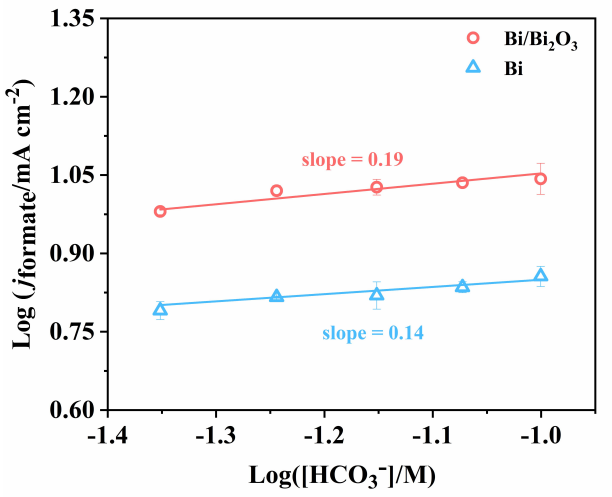


**Fig. S17.** $HCO_3^-$ concentration dependence of $j_{formate}$ in the presence of Bi NSs and $Bi/Bi_2O_3$ hybrid NSs at −0.96 V.

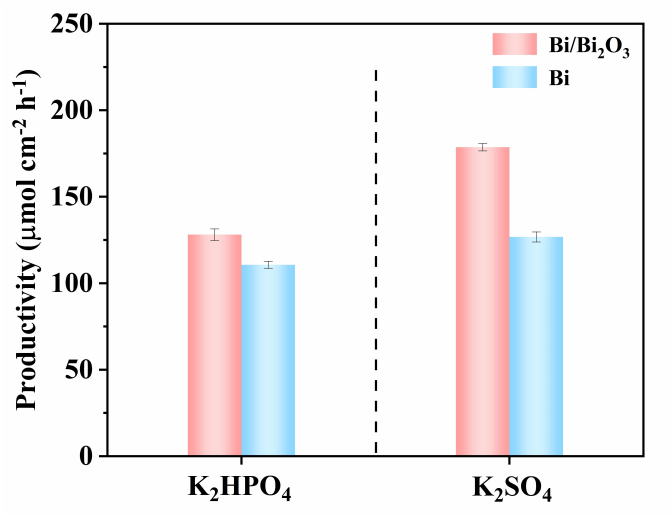


**Fig. S18.** Formate productivity obtained in the presence of Bi NSs and $Bi/Bi_2O_3$ hybrid NSs in different electrolytes at −0.96 V.

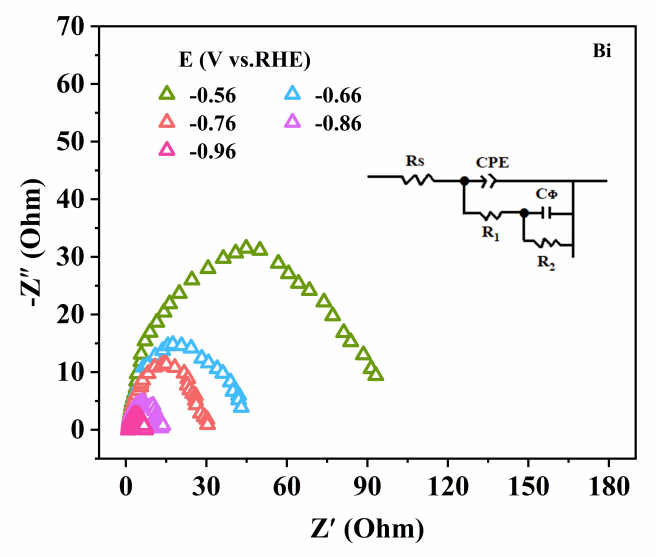


**Fig. S19.** Nyquist plots of Bi NSs.

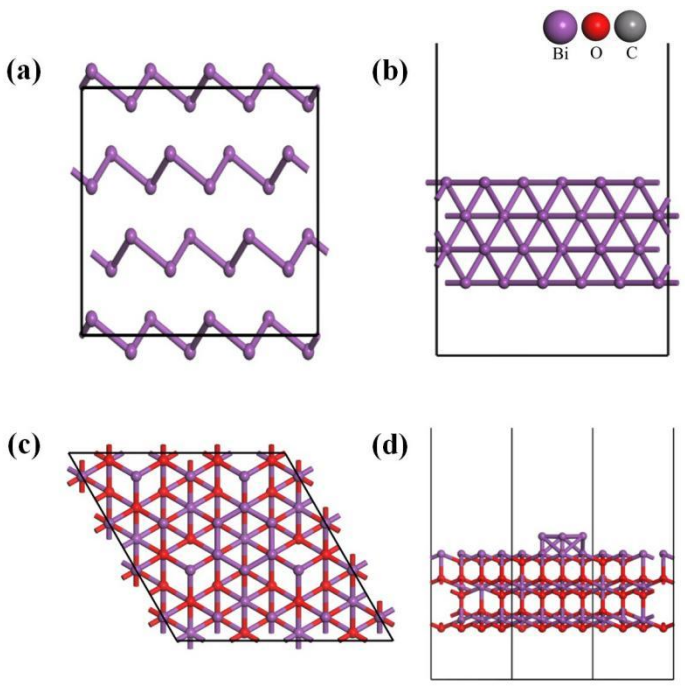


**Fig. S20.** Calculation models of the Bi slab (a top view, b side view) and Bi/$Bi_2O_3$ slab (c top view; d side view). The models of the Bi and Bi/$Bi_2O_3$ were performed on Bi (110) facet and $Bi_2O_3$ (222) facet since they were the predominantly exposed crystal plane on Bi and $Bi_2O_3$ NSs, respectively.

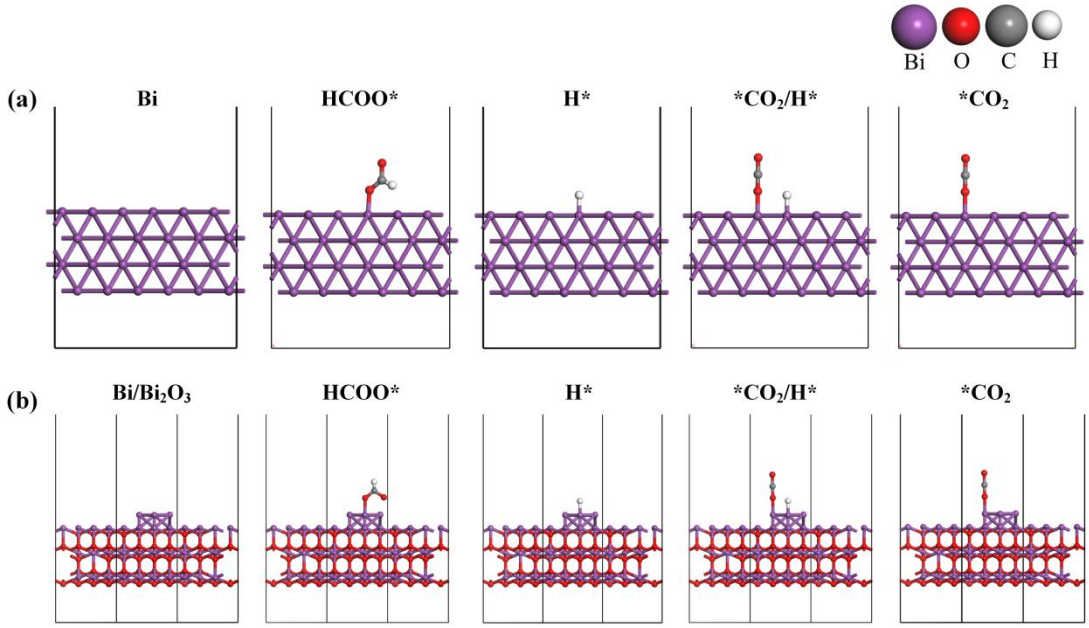


**Fig. S21.** Optimized geometric structure models of the intermediates adsorbed on (a) Bi, and (b) $Bi/Bi_2O_3$.

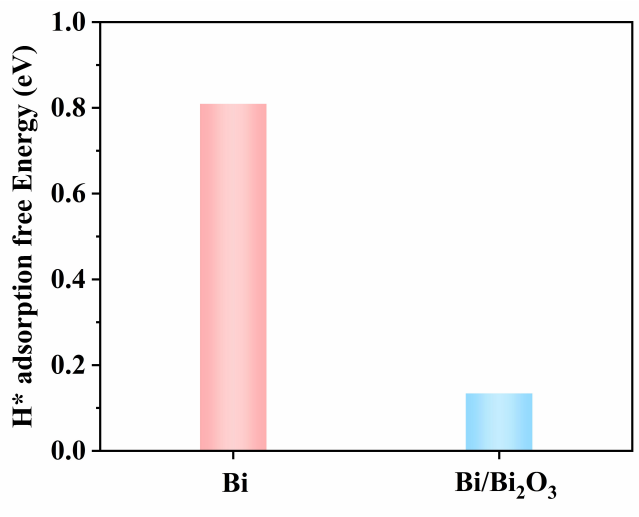


**Fig. S22.** The adsorption energy of H* on Bi and $Bi/Bi_2O_3$.

**Notes and references**

[1] F. Ke, Y. Jia, Y. F. Ji, P. Y. Kuang, B. C. Zhu, X. Y. Liu and J. G. Yu, *Acs. Catal.,* 2020, 10, 358.

[2] Q. Gong, P. Ding, M. Xu, X. Zhu, M. Wang, J. Deng, Q. Ma, N. Han, Y. Zhu, J. Lu, Z. Feng, Y. Li, W. Zhou and Y. Li, *Nat. Commun.,* 2019, 10, 2807.

[3] S. B. Liu, X. F. Lu, J. Xiao, X. Wang and X. W. Lou, *Angew. Chem.,* 2019, 58, 13828.

[4] H. Yang, N. Han, J. Deng, J. Wu, Y. Wang, Y. Hu, P. Ding, Y. Li, Y. Li and J. Lu, *Adv. Energy. Mater.,* 2018, 8, 1801536.

[5] P. L. Deng, F. Yang, Z. T. Wang, S. H. Chen, Y. Z. Zhou, S. Zaman and B. Y. Xia, *Angew. Chem.,* 2020, 59, 10807.

[6] P. L. Deng, F. Yang, Z. T. Wang, S. H. Chen, Y. Z. Zhou, S. Zaman and B. Y. Xia, *Angew. Chem.,* 2020, 59, 10807.

[7] Y. Zhang, R. Zhang, F. F. Chen, F. F. Zhang, Y. D. Liu, X. Y. Hao, H. K. Jin, X. H. Zhang, Z. M. Lu, H. Dong, F. Lu, W. H. Wang, H. Liu, H. Liu and Y. H. Cheng, *Appl. Catal. B.,* 2022, 322, 122127.

[8] P. L. Lu, D. L. Gao, H. Y. He, Q. X. Wang, Z. J. Liu, S. Dipazir, M. L. Yuan, W. Y. Zu and G. J. Zhang, *Nanoscale,* 2019, 11, 7805.

[9] Y. Wang, Y. Li, J. Liu, C. Dong, C. Xiao, L. Cheng, H. Jiang, H. Jiang and C. Li, *Angew. Chem.,* 2021, 60, 7681.

[10] P. L. Deng, F. Yang, Z. T. Wang, S. H. Chen, Y. Z. Zhou, S. Zaman and B. Y. Xia, *Angew. Chem.,* 2020, 59, 10807.

[11] F. Li, G. H. Gu, C. Choi, P. Kolla, S. Hong, T. S. Wu, Y. L. SOO, J. Masa, S. Mukerjee, Y. S. Jung, J. S. Qiu and Z. Sun, *Appl. Catal. B.,* 2020, 277, 119241.

[12] P. Liu, H. L. Liu, S. Zhang, J. Wang and C. Wang, *J. $CO_2$. Util.,* 2021, 51, 101643.

[13] S. Liu, Y. Fan, Y. Wang, S. Jin, M. Hou, W. Zeng, K. Li, T. Jiang, L. Qin, Z. Yan, Z. Tao, X. Zheng, C. Shen, Z. Liu, T. Ahmad, K. Zhang and W. Chen, *Nano. Lett.,* 2022, 22, 9107.

[14] H. Xie, T. Zhang, R. K. Xie, Z. F. Hou, X. C. Ji, Y. Y. Pang, S. Q. Chen, M. M. Titirici, H. M. Weng and G. L. Chai, *Adv. Mater.,* 2021, 33, 2008373.

[15] S. S. He, F. L. Ni, Y. J. Ji, L. Wang, Y. Z. Wen, H. P. Bai, G. J. Liu, Y. Zhang, Y. Y. Li, B. Zhang and H. S. Peng, *Angew. Chem.,* 2018, 57, 16114.

[16] P. Lamagni, M. Miola, J. Catalano, M. S. Hvid, M. A. H. Mamakhel, M. Christensen, M. R. Madsen, H. S. Jeppesen. X. M. Hu, K. Daasbjerg, T. Skrydstrup and N. Lock, *Adv. Funct. Mater.,* 2020, 30, 1910408.

[17] D. Wu, G. Huo, W. Chen, X. Z. Fu and J. L. Luo, *Appl. Catal. B.,* 2020, 271, 118957.

[18] Z. Z. Zhang, Z. W. Pan, Y. F. Guo, P. K. Wong, X. J. Zhou, R. B. Bai, *Appl. Catal. B.,* 2020, 261, 118212.

[19] P. F. Sui, C. Xu, M. N. Zhu, S. Liu, Q. Liu and J. L. Luo, *Small,* 2022, 18, 2105682.